Macromolecules

pubs.acs.org/Macromolecules Article

Layered Thin-Film Deposition via Extreme Inter-Brush Slip in a Lamellar Block Copolymer

Wenpeng Shan, Inbal Weisbord, Xueyan Feng, Jinho Hyon, Gkreti-Maria Manesi, Apostolos Avgeropoulos, Tamar Segal-Peretz,* and Edwin L. Thomas*

Cite This: https://doi.org/10.1021/acs.macromol.2c01496 Read Online

ACCESS | Metrics & More | Article Recommendations | Supporting Information

ABSTRACT: Creating ultrathin films via ballistic impact-induced frictional material transfer could be a new approach for additive manufacturing compared with current solvent-assisted polymer coatings. The covalently bonded A block brushes and B block brushes are robust mechanical units in A/B lamellar diblock copolymers (BCPs). The parallel brush−brush interfaces with low entanglement density present a unique set of slip planes that can undergo extreme deformation by shearing and delamination by tensile forces. Impact of microspheres comprised of concentric glassy−rubbery brush layers against a rigid substrate at ballistic strain rates causes adiabatic shock heating that permits compressional thinning of the bottommost layers via slip over both types of BCP brushes. In cooler regions, the mechanical contrast between the glassy A blocks and rubbery B blocks induces extensive slip across the rubbery block brushes. For angled impacts, the increased shear stress enhances brush slip and the particle slides across the substrate accompanied by delamination across the slip planes and unique frictional transfer of discrete A-block-B B-block-A layers.

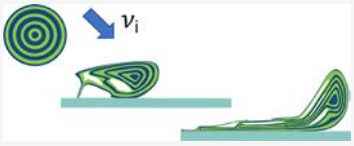

INTRODUCTION

Nanometer thin 2D layered materials such as graphite readily transfer to substrates via mechanical forces due to the low friction between the atomically flat layers.[1−3] Solvent-swollen polymer brushes also exhibit very low friction that is essential, for example, in the articulation of bone joints.[4,5] Lamellar block copolymers (BCPs) are a type of layered material having a smectic A liquid crystal structure with 1D translational order. Subjecting a bulk lamellar BCP sample to low-rate, high-temperature, large amplitude oscillatory shear results in global alignment with the lamellar normal parallel to the velocity gradient due to easy shear as well as delamination across the mid-layer brush−brush slip planes.[6,7] When subjected to forces normal to the layers, a chevron pattern of sharp kink boundaries forms parallel to the force axis.[8−11] For glassy−rubbery lamellar BCPs deformed at quasi-static strain rates and room temperature, the lamellar normal tilts away from the force direction with increased strain. When the applied force is at 45° to the lamellar normal, asymmetric kink boundaries form parallel to the force axis, while for tensile deformation parallel to the layers, the glassy layers fragment via a necking process.[9,10] Whether these various deformation mechanisms can take place in a lamellar BCP at the extreme rates characteristic of ballistic impact and how the relative magnitude of the normal vs the tangential stresses on the slip plane can affect the various deformation modes and whether material transfer of layers to a substrate can take place are essentially unexplored to date.

The laser-induced projectile impact test (LIPIT) has recently emerged as a useful small-scale ultrahigh strain rate test.[12] LIPIT has several loading configurations including particle-specimen impacts onto rigid substrates.[13−16] Quantitative studies are performed by monitoring the changes in the specimen-projectile speed and shape along with post-impact cross-sectional imaging of the specimen interior morphology. A simple initial microstructural state allows detailed analysis of the deformation mechanisms via post-impact microscopy of the deformation texture and displacement field of the material. In LIPIT, the impact event time scale is on the order of 10−100 ns. At this short time scale, the rapid heating from adiabatic shock can bring the polymer to temperatures well above the glass transition temperature (T_g) of the glassy component allowing visco-plastic flow, resulting in large deformations.[15] Fast cooling below the T_g arrests the material in a highly deformed state. A recent study of polystyrene-*block*-polydimethylsiloxane (PS-*b*-PDMS) impacted a specimen projectile at an angle Θ into a rigid substrate. This test, called Θ-LIPIT,[17] probed the tribological response by the addition of a tangential shear loading component, resulting in an increase in the frictional forces. Despite impacting at Θ = 45° at high velocities, all particles rebounded from the substrate without any noticeable polymer deposition. This behavior was likely due to the highly irregular microdomain structures, resulting in the lack of a set of well-defined slip planes in the PS-*b*-PDMS projectiles.[17]

Received: July 19, 2022
Revised: September 3, 2022

https://doi.org/10.1021/acs.macromol.2c01496
Macromolecules XXXX, XXX, XXX−XXX

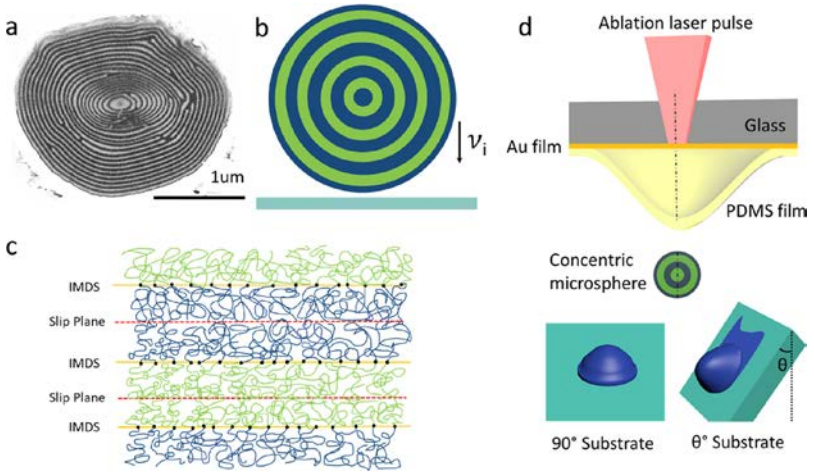

Figure 1. Initial microparticle specimen projectile. (a) A cross section of a microparticle made using FIB and imaged by SEM showing the concentric layers of PS (dark) and PDMS (bright). (b) Cross-sectional schematic. PS layers are dark blue and PDMS layers are light green in this and all other schematics. (c) Enlarged schematic of the molecular packing within the undeformed layers. The covalent junctions (dots) connecting the PS and PDMS blocks are located on the IMDS. The two sets of polymer brushes come into contact at the respective mid-layer slip planes. (d) Θ-LIPIT schematic of 90° and Θ° LIPIT impacts of BCP concentric microspheres.

Here, we show that concentric layered particles having well-defined slip planes can transfer a thin, continuous multi-stepped lamellar film onto the substrate when undergoing angled impact at high velocity. The precisely structured microparticles are created by 3D confinement of a lamellar-forming BCP in micron-sized spherical emulsion droplets. The solvent−BCP solution droplets are suspended within an immiscible fluid matrix[18] (see Methods), and very slow solvent dissolution into the surrounding water matrix results in a PS-*b*-PDMS concentric glassy ($T_{g\text{-PS}}$ ∼105 °C) and rubbery ($T_{g\text{-PDMS}}$ ∼−125 °C) layers. Microspheres are 2−3 microns in diameter, consisting of about 20−30 shells with an average shell thickness (lamellar period, d_0) of 50 nm. Individual microparticles were launched at velocities v_i from 300 to 600 m/s using Θ ranging from 90 to 45° to impact gold-covered silicon substrates. Incident projectile velocities were determined from images of the sphere taken just prior to impact superimposed onto a CCD camera using two laser pulses with a known time delay between them. Focused ion beam (FIB) milling and low-voltage scanning electron microscopy (SEM) of the cross sections of impacted and adhered particles along with SEM and atomic force microscopy (AFM) transferred films (Figure S1) permit detailed mapping of the changes in the thicknesses and shapes of the lamellar brush layers and insight into the conditions for material transfer at ultrahigh strain rates.

■ RESULTS AND DISCUSSION

Initial Spherical Projectile Morphology. The SEM image in Figure 1a shows a near-diametrical cross section of a microparticle exhibiting alternating concentric layers of PS (dark) and PDMS (bright). The idealized concentric spherical shell model is shown in Figure 1b with the corresponding molecular-scale schematic of the brushes with the covalent junctions between blocks located on the inter-material dividing surface (IMDS) and the two types of brush−brush mid-layer slip planes, shown in Figure 1c. The emulsion fabricated micron-sized spheres can have either PS or PDMS centers but always have a $^1/_2$ layer thickness of PS at the particle external surface due to the favorable surface interaction of the PS block with the polyvinyl alcohol surfactant−water matrix during sphere formation. Deformation by layer slip, kink boundary formation, and delamination depend on entanglements. There are two types of entanglements possible for each block. Intra-brush entanglements occur near the IMDS between adjacent blocks, and inter-brush entanglements can occur in the interdigitated mid-layer region.[19,20] By choosing a 42−32 kDa PS−PDMS diblock, we limit the number of entanglements across the slip planes. For these molecular weights, there would be approximately three entanglements per block, assuming that the respective blocks were in their homopolymer melts.[21] However, in the microphase-separated BCP, the entanglements are predominately intra-brush types, located closer to the IMDS with relatively few inter-brush entanglements near the mid-plane of each bilayer,[22] suggesting that the covalently bonded PS brushes and PDMS brushes will be robust units in the deformation and yet afford easy brush−brush slip across their mid-layers.[6,7,23]

Impacted Sphere Morphologies. Deformation depends on the particle's incident velocity v_i and angle of impact Θ to the substrate. For particles with a v_i <350 m/s, the BCP microsphere bounces off regardless of the impact angle, consistent with the behavior of many materials impacting a rigid substrate at low velocity and the earlier Θ-LIPIT investigation on PS-*b*-PDMS.[17] For v_i = 360 m/s, 90° impact, the particle adheres and deforms into an axisymmetric bell shape (Figure 2) with a smooth, round, upper surface that transitions to a broad flattened bottom region. Cross-sectional images show that the layers in the top portion of the projectile remain approximately concentric and circular with an average layer period d_0 equal to that of the original material, consistent with the external profile shape of the top portion as an undeformed spherical cap. The deformation creates a sharp axisymmetric mechanical tilt boundary from the original sphere center extending along the diagonal to the outermost peripheral edge and separating the highly deformed bottom portion from the less deformed upper region (Figure 2c). Since a particular shell volume and shell IMDS area strongly decrease with a decrease in the shell radius, the shells nearer the particle center must deform more extensively. Thus, the greatest layer

https://doi.org/10.1021/acs.macromol.2c01496
Macromolecules XXXX, XXX, XXX−XXX

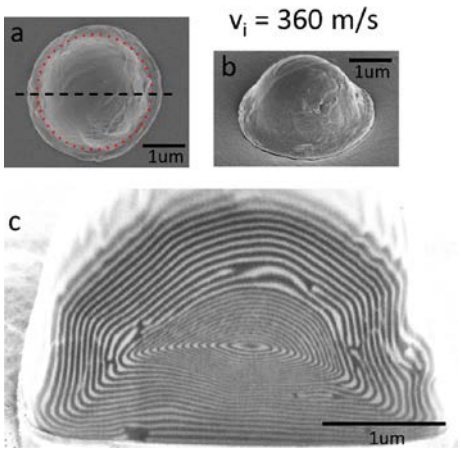

Figure 2. Spheres impacted at 90° for v_i = 360 m/s. Top (a), tilted (b), and cross-sectional SEM images (c) showing gradients in layer thickness and in spacing of the layers along the kink boundary that extends from the sphere center to the outer bottom periphery.

thinning takes place in the region just below the particle center. Depending on the impact velocity and location within the particle, the deformed layer period d can be as small as ~20 nm, indicating a very large compression ratio (d_0/d) over ~250%. Strong gradients in layer thickness, layer shape, and layer orientation develop due to the variation of the local loading state and the systematic variation of the layer circumference and orientation of the concentric shells.

With increased v_i, at 90° impact, the particle becomes even more flattened, with greater lateral area and an overall lens-like shape (see Figure 3). As occurs for the lower-velocity impacts, a prominent kink boundary spans from the sphere center radially outward to the bottom periphery. The upper surface shows one or sometimes two step-like features, usually asymmetrically shifted off-center, arising from additional pairs of kink boundaries (orange arrows in Figure 3c). At the highest velocity (v_i ~600 m/s), there are strong gradients in the shell thickness along the normal to the substrate and along the kink boundary. The average strain rate (see the SI, Section 5) is estimated to be ~10^7 s^{-1}. The impact severely compresses the layers approaching the particle center, making it difficult to distinguish individual layers in the SEM image, while closer to the substrate, the thicker layers can be resolved (Figure 3c). The layer repeat along the kink boundary near the center has increased by ~500%, while at the periphery, the increase is ~30%. Due to the greater mechanical contrast between the PS and PDMS in regions where the temperature rise due to adiabatic heating and viscous work is more modest, increased deformation along the kink boundary occurs by lateral separation of sets of nested shells due to mid-brush delamination exclusively within the more mobile, low T_g PDMS layers. The separation takes place by the successive pulling apart of the PDMS bilayer brushes, followed by fusing of the remaining PDMS brush to reform the PDMS bilayer. The pulling apart occurs via nucleation of pairs of $+^1/_2$ and $-^1/_2$ circular disclination loops within a given PDMS layer (see Figure 3d). Due to the successively smaller shell circumference approaching the particle center, the slip distance between the opposite sign disclination cores must increase approaching the particle center. In the upper region of the deformed particle where the temperature rise is relatively lower, the PS layers show local thinning characteristic of necking. At the top center of the deformed particle associated with the small dimple region, layer bucking appears, likely due to the partial retraction of the expanded, necked layers after particle arrest (see the large blue arrow in Figure 3c). Annealing of impacted particles (150 °C, 1 h) demonstrates that the highly compressed blocks reorganize into considerably fewer shells having the original ~50 nm period thickness, but since the overall particle shape stays as a flattened disc, the kink boundary remains (Figure S7a,b). Overall, at sufficient impact velocity, the spheres deform and adhere to the substrate but present a relatively thick, nonuniform structure.

To enhance the possibility for layer transfer and film formation on the substrate, spheres were impacted at Θ of 70, 55, and 45°. Now, the deformed shape of the particle is no longer axisymmetric due to the increased tangential velocity component inducing more unidirectional shearing (Figures 4−6 and Figure S2). Since the compressional forces are lower, lateral spreading and particle adhesion are less and the tensile

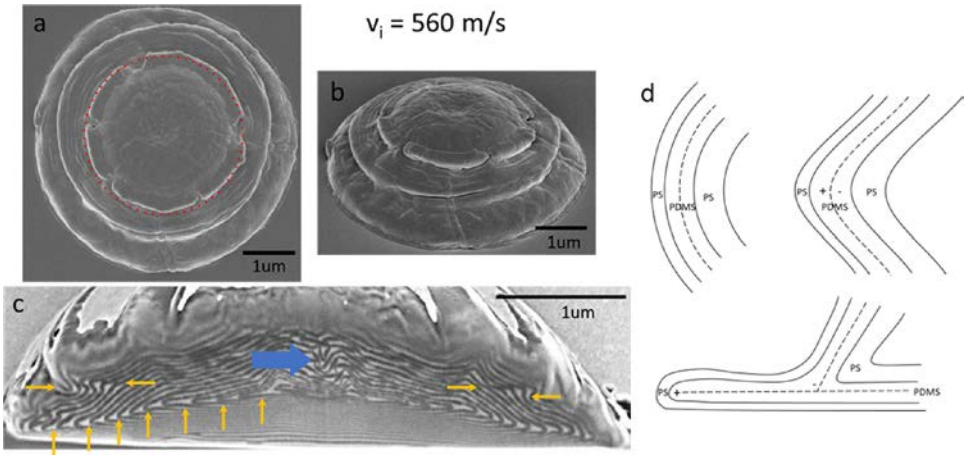

Figure 3. Spheres impacted at 90° for v_i = 560 m/s. Top (a), tilted (b), and cross-sectional SEM images (c). The surface steps evident in the topmost particle region (a, b) are due to the formation of pairs of kink boundaries, as observed in (c) (denoted by pairs of horizontal orange arrows). The cross section in (c) shows the prominent radial kink boundary (vertical orange arrows) with the expanded layer spacing along the boundary greatest near the particle center. PS layer buckling and necking occur due to partial layer recovery in the central top region (blue arrow). (d) Schematic depicting the nucleation of $+^1/_2$ and $-^1/_2$ disclination loop pairs within the PDMS layers along the kink boundary.

https://doi.org/10.1021/acs.macromol.2c01496
Macromolecules XXXX, XXX, XXX−XXX

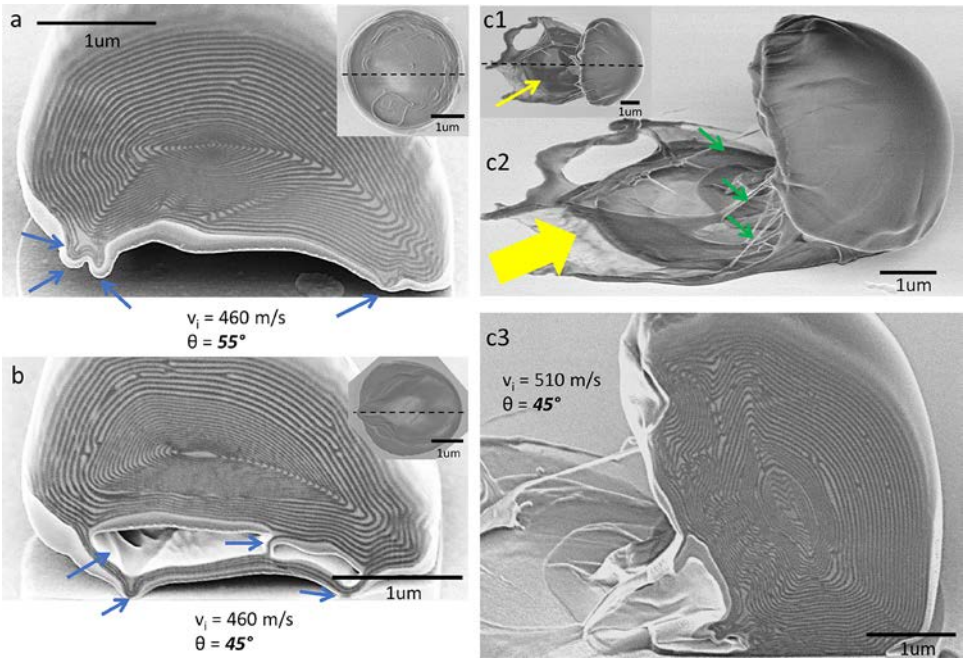

Figure 4. Θ-LIPIT particle impacts and friction-induced stepped layer transfer to the substrate. Top views (small insets) and cross-sectional SEM images of impacted spheres for Θ of 55° (a) and 45° (b, c). Particles exhibit a kink boundary running from the center to the periphery. The blue arrows in (a, b) point to the bottom regions of the particle that were or are still adhering to the substrate and, as the particle tried to rebound, caused tensile stresses accompanied by delamination−cavitation within the bottommost PDMS layers. (c) At higher impact velocities, Θ = 45° particles slide over the substrate depositing ultra-sheared layers (yellow arrows). The layers are connected to the mushroom-shaped particle cap by long fibril ribbons (green arrows) drawn from the layers. (c3) Higher magnification cross-sectional image of the rotated cap region showing the formation of multiple kink boundaries. The bottom layers successively experience compression and strong shear and then tension as the particle tries to rebound from the surface.

rebound force normal to the flattened bottom layers can induce local detachment of the particle from the substrate, along with layer expansion, delamination, and cavity formation (observed exclusively between the PDMS brushes (Figure 4b)). However, most interestingly, for 55 and 45° impacts at the highest velocities, large regions of the substrate become covered with a thin polymer film. Here, frictional shear forces cause layers to adhere to the substrate via slip and pull out of a complete PS bilayer with its surrounding upper and lower PDMS brushes (i.e., one lamellar repeat unit: PDMS-*b*-PS PS-*b*-PDMS). As a result, the substrate becomes covered with a stepped multilayer film with discrete, individual deformed layer period steps in height (Figure 5c and Figure S9). This unique deformation behavior is very different from that of quasi-static deformation of lamellar BCPs[9,10] as well as the prior LIPIT research.[17] Indeed, in the previous research on PS-*b*-PDMS particles (with approximately 2× higher molecular weight blocks and disorganized, irregularly shaped microdomains), 100% of the 45° impacts at similar v_i rebounded from the substrate without leaving any adhering polymer due to the lack of well-defined slip planes within the projectiles. On the other hand, with particles having well-defined slip planes and low entanglements across these slip planes, layer transfer and continuity readily occur.

Numerous highly drawn ribbon fibrils extend from the adhered film and arrest the (often rotated) particle (Figures 4c and 5a and Figure S8). Figure 5b shows the cross-sectional schematic of the nested and laterally displaced shells with the appearance of the positive and negative $^1/_2$ disclination lines due to the delamination of adjacent PDMS brushes and subsequent extensive slip (e.g., in Figure 5b, the PDMS layer is pulled away and typically slips a fraction of a micron distance over the neighboring PDMS brush, allowing the upper and lower parts of the PDMS layer to fold toward each other and fuse together). Surprisingly, the ribbon fibrils are comprised of thinned but unmixed PS and PDMS layers, suggesting that the pair of A and B block brushes covalently connected across the IMDS act as a robust unit in the deformation (Figure S4). This behavior is contrary to that accepted for quasi-static room temperature deformation of glassy BCP lamellae where a craze fibril morphology forms in the plane of the lamella with the chains assumed to have become mixed and oriented parallel to the fibril axis with fibril extension ratios of around 400%.[24] These novel layered ribbon fibrils can exhibit high (many 100 s %) extension ratios and with only a small amount of recovery, as evidenced by their small retraction after failure (Figure S5).

Whether a homogeneous and oriented mixture of the two blocks occurs within the ribbon fibrils and the deposited layers depends on the nature of the deformation units and on the degree of segregation. The segment−segment interaction parameter $\chi(T)$ between PS and PDMS is quite large, and for the 42−32 kDa BCP, the equilibrium order−disorder transition temperature (T_{ODT}) is estimated to be ∼1000 °C (calculation in the SI), suggesting that block mixing during deformation is highly unfavorable. However, the effective T_{ODT} during an impact event also depends on the pressure[28] as well as the imposed mechanical strain to the specimen.[29] Hydrostatic pressure generally raises the ODT due to an increase in the system volume upon mixing, while extensive layer deformation lowers the ODT due to the unfavorable chain conformations. Hydrocode simulations of particle impact to a glassy homopolymer PS at these velocities show that the

https://doi.org/10.1021/acs.macromol.2c01496
Macromolecules XXXX, XXX, XXX−XXX

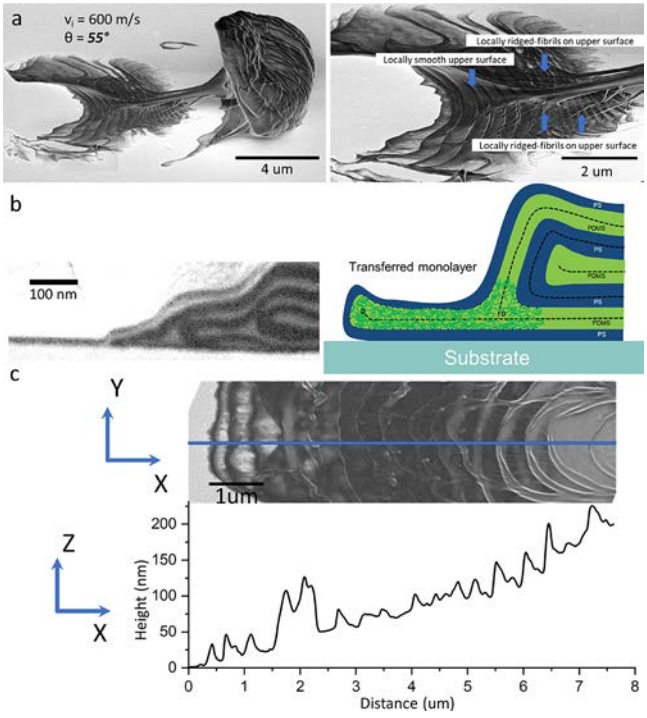

Figure 5. Friction-induced slip steps via layer deposition. (a) (Left) Top view SEM image of the arrested particle with ribbon fibrils connecting the adhered layers to the particle cap. (Right) Higher magnification showing details of the stepped surface of the deposited layers. (b) (Left) Cross-sectional SEM image of a set of deposited layers. (Right) Schematic of the laterally sheared peripheral region of the lamellar BCP showing the formation of a Grandjean terrace-like structure.[25−27] As a result, a $s = +^1/_2$ disclination is located at the initial delamination position, and a $s = -^1/_2$ disclination is positioned where the PDMS brushes rejoin. (c) SEM image and corresponding $z(x)$ height profile from an AFM image of the laterally displaced and drawn concentric layers deposited on the substrate via ultra-shear in the outer regions of a particle for 580 m/s impact at 45°. Drawn fibrils and elongated voids aligned along the shear direction are evident within the leftmost initial deposited layers.

compressive shock wave creates a several GPa step jump in pressure that is released within ∼100 ps[13]. The initial jump in temperature due to shock compression slightly lags that of the pressure rise. Importantly, the temperature can continue to rise with heating persisting for much longer times due to the substantial amount of visco-plastic work occurring in the deforming particle. Together, the initial shock compression and visco-plastic work rapidly heat the particle to an average particle temperature estimated to be ranging from 150 to 370 °C (SI, Section 2). High pressure also raises the T_g of the blocks, but due to the short high-pressure duration compared with the duration of the temperature increase, the T_g of each block will drop back to its ambient pressure value well before the specimen temperature falls. Thus, in regions of high deformation, both blocks will have good mobility during most of the impact event. The block polymer chains will tend to partially relax to relieve the strong alteration of the chain conformations, but the higher T_g PS domains freeze-in the highly deformed structure. The cross-sectional images showing the strongly altered domain dimensions and shapes within the adhered particle and across the transferred film (Figures 2−5 and Figures S2−S4) suggest that the blocks do not mix during deformation and film transfer. Moreover, without PS continuity and purity, a (partially) mixed and highly fragmented block structure could not resist the relaxation that would occur from a rather low effective T_g and/or discontinuous PS domains.

CONCLUSIONS

As evident from the analysis of the SEM micrographs and the AFM images of Θ-LIPIT experiments, the pair of block brushes covalently connected across the IMDS constitute a robust layered deformation unit that can undergo extensive shear over the lamellar brush−brush slip planes and undergo tensile delamination across the rubbery brush−brush layers under ultrahigh strain rate conditions. The primary deformation processes that take place are schematically depicted in Figure 6. The state of stress depends on v_i and Θ and on location and time. Impact of the particle results in initial adiabatic shock compression that elevates the sample temperature above the T_g of the PS block, allowing visco-plastic particle flattening and layer shear thinning over the intra-layer slip planes of both PS and PDMS. At normal incidence, the approximately axisymmetric lateral spread of the particle is accompanied by the formation of a radially oriented kink boundary, allowing the layers to flatten and become more parallel throughout the particle. The kink boundary exhibits a strong gradient in the length of the PDMS layers due to nucleation and lateral separation of pairs of $+^1/_2$ and $-^1/_2$ disclination loops within each rubbery PDMS layer. At low impact velocities, the kink boundary separates a more highly deformed lower region from a less deformed upper region (Figure 6a,b). Importantly, for off-normal impact, the enhanced lateral forces trigger large unidirectional shear by lateral displacement of the $-^1/_2$ disclination defects across the PDMS brush−brush slip planes. Additionally, tensile forces due to particle recoil and friction-induced particle rotation cause brush−brush delamination exclusively within the PDMS layers (Figure 6c,d). For high-velocity impacts at Θ = 55 and 45°, the facile brush−brush layer slip enables successive detachment of discrete PDMS-*b*-PS PS-*b*-PDMS layers from the particle as it slides across the substrate, leading to transfer of an ultrathin film with an initial thickness of a single lamellar period (∼50 nm) and steadily increased thickness in discrete single period steps across the substrate (Figures 5c and 6d and Figure S6). Overall, adiabatic heating-induced thermal softening during LIPIT enables the activation of the mid-layer brush slip planes, resulting in extensive energy dissipation via visco-plastic shear, tensile delamination, frictional deposition of layers, and drawing processes during impact without the usual deformation-induced chain orientation typical of polymeric materials. The possibility to use such particles with well-defined and easy slip planes for cold spray deposition of uniquely structured polymer coatings seems promising.

METHODS

Materials. The PS-*b*-PDMS diblock copolymer was synthesized by Dr. G.-M. Manesi in the group of Professor A. Avgeropoulos (Ioannina University, Greece) using sequential anionic polymerization of styrene and hexamethylcyclotrisiloxane according to procedures already reported in the literature.[30] The number average molecular weights are PS 42 kg/mol and PDMS 32 kg/mol, and the volume fraction of PDMS is approximately 45%, with a dispersity (Đ) of 1.04. The 5.1 μm pore diameter SPG (Shirasu Porous Glass) membrane was purchased from SPG Technology Co., Ltd.

Concentric Lamellar BCP Microsphere Fabrication. To form uniform-size microspheres, a microemulsion procedure established by

https://doi.org/10.1021/acs.macromol.2c01496
Macromolecules XXXX, XXX, XXX−XXX

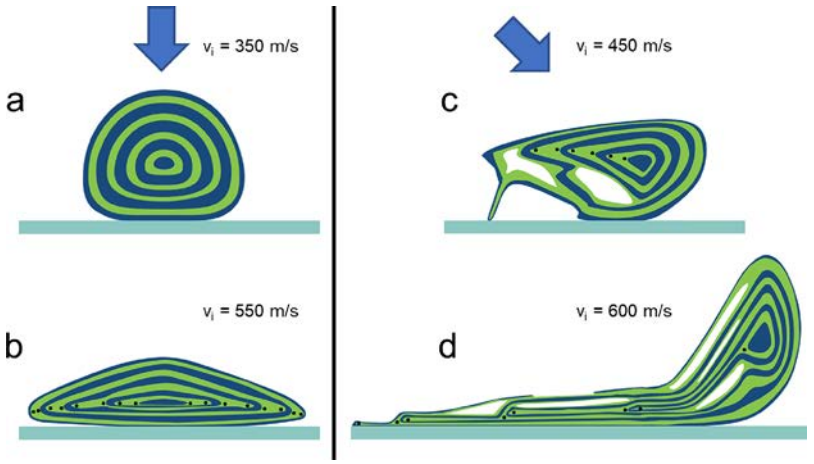

Figure 6. Schematics depicting the particle deformation. The morphological evolution of the concentric layered structure during impact of a microsphere depends on impact velocity and angle. (a, b) Normal impacts at ~350 and 550 m/s. (c, d) 45° impacts at ~450 and 600 m/s. For impacts at 90°, the layers undergo slip and the sphere takes on a flat bottom shape with highly thinned layers and an axisymmetric kink boundary. Pairs of disclination line loop defects (denoted by the black points) are nucleated exclusively in the PDMS layers and move apart by lateral slip over the brush−brush interfaces. For 45° impacts, a stepped polymer layer deposit is transferred to the substrate via friction (d). This results from PDMS (green) layer delamination, ultra-shearing across the PDMS brush slip planes (evidenced by the large lateral separation of the disclination pairs in the green layers). Ribbon fibrils drawn from the adhered layers arrest the particle. Unmixed PS and PDMS layers are maintained throughout the deformation.

Kim et al. was employed.[18] We used a 0.3 wt % block copolymer solution in chloroform to form the dispersed phase in DI water with polyvinyl alcohol (PVA; MW = 13−23 kg mol^{-1}, 87−89% hydrolyzed, purchased from Sigma-Aldrich) as the surfactant. With the help of nitrogen gas, the polymer and solvent (2 mL) were forced through a 5.1 micron pore diameter SPG membrane, forming a narrow size distribution of microspheres stabilized by the surfactant. Subsequently, the beaker containing the particles was left open for at least 12 h at 30 °C to completely remove the chloroform via slow dissolution into the water and then evaporation from the water surface. To remove the PVA surfactant, the solid microspheres were washed, centrifuged at 11,000 rpm for 8 min, and redispersed in DI water three times.

Slice and View SEM. A high-energy Ga^+ ion beam (30 keV, 80 pA) was used to mill away a section of a particle, and then a low-energy electron beam (1 keV, 50 pA) was directed at the surface and a secondary-electron image recorded (Figure S1) via a through lens (TLD) secondary-electron detector. The excellent ion milling behavior and the intrinsic large difference of the low-voltage secondary electron emission between the silicon-containing PDMS regions (bright) and the hydrocarbon PS regions (dark) allows for detailed cross-sectional visualization and analysis of the deformed microparticles. Before milling the FIB cross sections, the impacted particle was first coated with a protective layer of Pt-C.

AFM. Tapping mode on a multimode AFM (Bruker's Dimension Icon) was used to probe the height profiles of deposited layers and roughness of the substrate. Data were processed using Gwyddion software.

Launch Pad Preparation. The launch pad used for shooting the microparticle projectiles is similar to previous LIPIT studies.[31] The polymer microspheres suspended in water were drop cast onto the launch pad and spread across the surface via a standard lab wipe (Kimberly-Clark Kimwipe).

■ ASSOCIATED CONTENT

Supporting Information

The Supporting Information is available free of charge at https://pubs.acs.org/doi/10.1021/acs.macromol.2c01496.

Additional experimental details, related calculations, and extra schematic, SEM, and AFM images (PDF)

■ AUTHOR INFORMATION

Corresponding Authors

Tamar Segal-Peretz − *Department of Chemical Engineering Technion, Israel Institute of Technology, Haifa 32000, Israel;* orcid.org/0000-0003-3222-6429; Email: tamarps@technion.ac.il

Edwin L. Thomas − *Department of Materials Science and Engineering, Texas A&M University, College Station, Texas 77840, United States;* orcid.org/0000-0001-5911-6524; Email: elt@tamu.edu

Authors

Wenpeng Shan − *Department of Materials Science and Engineering, Texas A&M University, College Station, Texas 77840, United States*

Inbal Weisbord − *Department of Chemical Engineering Technion, Israel Institute of Technology, Haifa 32000, Israel*

Xueyan Feng − *Department of Materials Science and Engineering, Texas A&M University, College Station, Texas 77840, United States*

Jinho Hyon − *Department of Materials Science and Engineering, Texas A&M University, College Station, Texas 77840, United States*

Gkreti-Maria Manesi − *Department of Materials Science and Engineering, University of Ioannina, University Campus-Dourouti, Ioannina 45110, Greece;* orcid.org/0000-0002-1225-1515

Apostolos Avgeropoulos − *Department of Materials Science and Engineering, University of Ioannina, University Campus-Dourouti, Ioannina 45110, Greece;* orcid.org/0000-0002-6203-9942

Complete contact information is available at: https://pubs.acs.org/10.1021/acs.macromol.2c01496

Author Contributions

W.S., I.W., T.S.-P., and E.L.T. conceived the concept and designed the experiments. W.S., I.W., X.F., G.-M.M., A.A., and

https://doi.org/10.1021/acs.macromol.2c01496
Macromolecules XXXX, XXX, XXX−XXX

J.H. performed the experiments, and all authors analyzed the data and participated in writing the manuscript.

Funding

This research was supported by the U.S.−Israel Binational Science Foundation grant no. 2020295 and a grant from NSF DMR-2105296.

Notes

The authors declare no competing financial interest.

■ ACKNOWLEDGMENTS

The authors thank Dr. K. Xiao of Texas A&M University (TAMU) and Professors J.-H. Lee and G. Grason of the University of Massachusetts for useful discussion. Mr. J. Shelton of TAMU contributed the schematic drawings.

■ REFERENCES

(1) Paton, K. R.; Varrla, E.; Backes, C.; Smith, R. J.; Khan, U.; O'Neill, A.; Boland, C.; Lotya, M.; Istrate, O. M.; King, P.; Higgins, T.; Barwich, S.; May, P.; Puczkarski, P.; Ahmed, I.; Moebius, M.; Pettersson, H.; Long, E.; Coelho, J.; O'Brien, S. E.; McGuire, E. K.; Sanchez, B. M.; Duesberg, G. S.; McEvoy, N.; Pennycook, T. J.; Downing, C.; Crossley, A.; Nicolosi, V.; Coleman, J. N. Scalable production of large quantities of defect-free few-layer graphene by shear exfoliation in liquids. *Nat. Mater.* **2014**, *13*, 624−630.

(2) Novoselov, K. S.; Geim, A. K.; Morozov, S. V.; Jiang, D.-e.; Zhang, Y.; Dubonos, S. V.; Grigorieva, I. V.; Firsov, A. A. Electric field effect in atomically thin carbon films. *Science* **2004**, *306*, 666−669.

(3) Peng, D.; Wu, Z.; Shi, D.; Qu, C.; Jiang, H.; Song, Y.; Ma, M.; Aeppli, G.; Urbakh, M.; Zheng, Q. Load-induced dynamical transitions at graphene interfaces. *Proc. Natl. Acad Sci.* **2020**, *117*, 12618−12623.

(4) Jahn, S.; Klein, J. Lubrication of articular cartilage. *Phys. Today* **2018**, *71*, 48−54.

(5) Lin, W.; Kluzek, M.; Iuster, N.; Shimoni, E.; Kampf, N.; Goldberg, R.; Klein, J. Cartilage-inspired, lipid-based boundary-lubricated hydrogels. *Science* **2020**, *370*, 335−338.

(6) Koppi, K. A.; Tirrell, M.; Bates, F. S.; Almdal, K.; Colby, R. H. Lamellae orientation in dynamically sheared diblock copolymer melts. *J. Phys. II* **1992**, *2*, 1941−1959.

(7) Patel, S. S.; Larson, R. G.; Winey, K. I.; Watanabe, H. Shear Orientation and Rheology of a Lamellar Polystyrene-Polyisoprene Block Copolymer. *Macromolecules* **1995**, *28*, 4313−4318.

(8) De Gennes, P.; Prost, J. *The Physics of Liquid Crystals*; Clarendon Press: Oxford 1993.

(9) Cohen, Y.; Albalak, R. J.; Dair, B. J.; Capel, M. S.; Thomas, E. L. Deformation of oriented lamellar block copolymer films. *Macromolecules* **2000**, *33*, 6502−6516.

(10) Cohen, Y.; Brinkmann, M.; Thomas, E. L. Undulation, dilation, and folding of a layered block copolymer. *J. Chem. Phys* **2001**, *114*, 984−992.

(11) Makke, A.; Perez, M.; Lame, O.; Barrat, J.-L. Nanoscale buckling deformation in layered copolymer materials. *Proc. Natl. Acad Sci.* **2012**, *109*, 680−685.

(12) Veysset, D.; Lee, J.-H.; Hassani, M.; Kooi, S. E.; Thomas, E. L.; Nelson, K. A. High-velocity micro-projectile impact testing. *Appl. Phys. Rev.* **2021**, *8*, No. 011319.

(13) Hyon, J.; Gonzales, M.; Streit, J. K.; Fried, O.; Lawal, O.; Jiao, Y.; Drummy, L. F.; Thomas, E. L.; Vaia, R. A. Projectile Impact Shock-Induced Deformation of One-Component Polymer Nanocomposite Thin Films. *ACS Nano* **2021**, *15*, 2439−2446.

(14) Chan, E. P.; Xie, W.; Orski, S. V.; Lee, J.-H.; Soles, C. L. Entanglement Density-Dependent Energy Absorption of Polycarbonate Films via Supersonic Fracture. *ACS Macro Lett.* **2019**, *8*, 806−811.

(15) Hyon, J.; Lawal, O.; Fried, O.; Thevamaran, R.; Yazdi, S.; Zhou, M.; Veysset, D.; Kooi, S. E.; Jiao, Y.; Hsiao, M.-S.; Streit, J.; Vaia, R. A.; Thomas, E. L. Extreme Energy Absorption in Glassy Polymer Thin Films by Supersonic Micro-projectile Impact. *Mater. Today* **2018**, *21*, 817−824.

(16) Cai, J.; Thevamaran, R. Superior Energy Dissipation by Ultrathin Semicrystalline Polymer Films Under Supersonic Micro-projectile Impacts. *Nano Lett.* **2020**, *20*, 5632−5638.

(17) Kim, A.; Müftü, S.; Thomas, E. L.; Lee, J.-H. Extreme Tribological Characteristics of Copolymers Induced by Dynamic Rheological Instability. *ACS Appl. Polym. Mater.* **2021**, *3*, 4413−4418.

(18) Shin, J. M.; Kim, M. P.; Yang, H.; Ku, K. H.; Jang, S. G.; Youm, K. H.; Yi, G.-R.; Kim, B. J. Monodipserse Nanostructured Spheres of Block Copolymers and Nanoparticles via Cross-Flow Membrane Emulsification. *Chem. Mater.* **2015**, *27*, 6314−6321.

(19) Pan, X.; Shaffer, J. S. Onset of Chain Entanglements in Block Copolymer Lamellae. *Macromolecules* **1996**, *29*, 4453−4455.

(20) Joanny, J. F. Lubrication by molten polymer brushes. *Langmuir* **1992**, *8*, 989−995.

(21) Fetters, L. J.; Lohse, D. J.; Richter, D.; Witten, T. A.; Zirkel, A. Connection between Polymer Molecular Weight, Density, Chain Dimensions, and Melt Viscoelastic Properties. *Macromolecules* **1994**, *27*, 4639−4647.

(22) Sethuraman, V.; Kipp, D.; Ganesan, V. Entanglements in Lamellar Phases of Diblock Copolymers. *Macromolecules* **2015**, *48*, 6321−6328.

(23) Polis, D. L.; Winey, K. I. Controlling kink band morphology in block copolymers: Threshold criteria and stability. *Macromolecules* **1998**, *31*, 3617−3625.

(24) Lee, J.-Y.; Crosby, A. J. Crazing in Glassy Block Copolymer Thin Films. *Macromolecules* **2005**, *38*, 9711−9717.

(25) Friedel; Grandjean, F. *Bull. Soc. Fr. Miner.* **1910**, *33*, 192.

(26) Kléman, M. Defects in liquid crystals. *Rep. Prog. Phys.* **1989**, *52*, 555.

(27) Kleman, M.; Friedel, J. Disclinations, dislocations, and continuous defects: A reappraisal. *Rev. Mod. Phys.* **2008**, *80*, 61.

(28) Hajduk, D. A.; Gruner, S. M.; Erramilli, S.; Register, R. A.; Fetters, L. J. High-Pressure Effects on the Order−Disorder Transition in Block Copolymer Melts. *Macromolecules* **1996**, *29*, 1473−1481.

(29) Lee, J. H.; Veysset, D.; Singer, J. P.; Retsch, M.; Saini, G.; Pezeril, T.; Nelson, K. A.; Thomas, E. L. High strain rate deformation of layered nanocomposites. *Nat. Commun.* **2012**, *3*, 1164.

(30) Politakos, N.; Ntoukas, E.; Avgeropoulos, A.; Krikorian, V.; Pate, B. D.; Thomas, E. L.; Hill, R. M. Strongly segregated cubic microdomain morphology consistent with the double gyroid phase in high molecular weight diblock copolymers of polystyrene and poly(dimethylsiloxane). *J. Polym. Sci., Part B: Polym. Phys.* **2009**, *47*, 2419−2427.

(31) Lee, J.-H.; Loya, P. E.; Lou, J.; Thomas, E. L. Dynamic mechanical behavior of multilayer graphene via supersonic projectile penetration. *Science* **2014**, *346*, 1092−1096.

https://doi.org/10.1021/acs.macromol.2c01496
Macromolecules XXXX, XXX, XXX−XXX